Evidence of high-spin Ru and universal magnetic anisotropy in $SrRuO_3$ thin films

A. J. Grutter,[1,2] F. J. Wong,[1] E. Arenholz,[3] A. Vailionis,[4,5] and Y. Suzuki[1,2,4]

[1]*Department of Materials Science and Engineering, University of California, Berkeley, California 94720, USA*

[2]*Materials Sciences Division, Lawrence Berkeley National Laboratory, Berkeley, California 94720, USA*

[3]*Advanced Light Source, Lawrence Berkeley National Laboratory, Berkeley, California 94720, USA*

[4]*Geballe Laboratory for Advanced Materials, Stanford University, Stanford, California, 94305, USA*

[5]*Stanford Institute for Materials and Energy Sciences, SLAC National Accelerator Laboratory, Menlo Park, California 94025, USA*

(Received 7 November 2011; revised manuscript received 21 March 2012; published 17 April 2012)

We have investigated the origins of enhanced saturated magnetic moment and strong strain-dependent magnetic anisotropy in epitaxial films of the transition-metal oxide $SrRuO_3$. We find evidence for an enhancement of the carrier concentration and the stabilization of high-spin Ru^{4+}. Through x-ray magnetic circular dichroism measurements, we also observe a strain-dependent enhancement of the out-of-plane orbital magnetic moment. Such an enhancement is consistent with the universal out-of-plane anisotropy axis shown to occur in films in a variety of different crystallographic orientations. We explain all these effects in terms of an anisotropic reduction in the crystal field resulting from anisotropically reduced orbital overlap in distorted films.

DOI: 10.1103/PhysRevB.85.134429 PACS number(s): 75.70.Ak, 75.30.Gw, 73.20.At

I. INTRODUCTION

Structural distortions give rise to modifications in electronic structure that can stabilize novel electronic and magnetic ground states. Transition-metal complex oxides, with widely varying properties and strongly correlated electronic interactions, offer exciting model systems in which to study the stabilization of these new ground states via lattice distortions.[1–3] Recent advances in deposition techniques have allowed the development of atomically precise epitaxial complex oxide thin films. Thus, thin films of these materials are now being used to separate microstructural effects from those of interfaces and lattice distortions.

The ferromagnetic metal $SrRuO_3$ (SRO) is one such oxide that has attracted much attention. It is unique as the only known 4*d* transition-metal oxide ferromagnet. In most 4*d* systems, the extended orbitals increase the bandwidth and decrease the density of states at the Fermi level, precluding Stoner-type ferromagnetism.[4,5] In SRO, however, strong hybridization of the Ru 4*d* and O 2*p* bands enhances the density of states at the Fermi level, resulting in ferromagnetic interactions and metallicity.[6–8] Consequently, bulk SRO exhibits strong magnetism for a 4*d* system, with a bulk Curie temperature (T_C) of 160 K and reported saturated moment values ranging from 1.1 to 1.6 μ_B/Ru^{4+}.[7,9–11] Due to the large crystal field splitting, Ru^{4+} ions are usually expected to be in a low-spin state with an electron configuration of t_{2g}^4 ($3\uparrow$, $1\downarrow$) corresponding to 2 μ_B/Ru^{4+} ion—higher than what is experimentally observed. The lower experimental values of Ru moment in SRO thus far have been attributed to electron delocalization associated with itinerancy.[7] Until recently, there had been no report of a Ru-based compound with a high-spin-state (4 μ_B/Ru^{4+}) ion.

Thin films of SRO have been shown to exhibit highly tunable, non-bulk-like properties. Studies of SRO films have reported a metal-insulator transition, competition between ferromagnetic and antiferromagnetic states in ultrathin films, and spin-glass behavior.[12–14] Since we demonstrated that epitaxial strain could be used to enhance the saturation magnetization (M_S) of SRO thin films, there have been several reports of similarly enhanced magnetic moment.[15–18] These experimental results, in which compressive strain enhanced the saturated moment, are at odds with theoretical studies where compressively strained (100) and (110) SRO films are predicted to have saturated magnetic moments suppressed from bulk values.[19] It is also predicted that an enhanced moment can be realized through the application of biaxial tension, although we are not aware of any experimental confirmation or contradiction of this prediction.[19]

Recent reports have also shown that when SRO thin films are grown on (100) and (110) $SrTiO_3$ (STO), they exhibit an out-of-plane (OOP) easy axis that is independent of crystallographic orientation.[14,18] That is, when grown on (100) STO, the film easy axis is in the [100] direction, but, when grown on (110) STO, the easy axis is in the [110] direction.[14,18] Additionally, the anisotropy is very strong, with different in-plane (IP) and OOP moments reported at applied fields of up to 5 T.[14,18]

In this paper, we demonstrate that both enhanced saturated magnetic moment and strong uniaxial anisotropy can be induced simultaneously through the application of compressive epitaxial strain. In (111)-oriented films, the resulting distortions of the Ru octahedral environment may cause electrons to populate the newly split e_g band, effectively placing the Ru in a high-spin state and enhancing the magnetic moment. We find an increase in the carrier concentration consistent with the presence of such high-spin Ru. SRO films grown under identical conditions on (100) and (110) substrates show similar behavior but are more consistent with a low-spin Ru state. All films with enhanced saturated moment also show strong uniaxial magnetic anisotropy with an OOP easy direction. By systematically varying the magnitude of the lattice distortions in the SRO samples, we conclusively show that these lattice distortions are the source of the enhanced Ru moment, larger carrier concentration, and strong magnetic anisotropy. We speculate that lattice distortions anisotropically alter the bonding in the Ru-O octahedra in a way that simultaneously reduces the quenching of the orbital moment and involves the e_g states in the magnetism, explaining all our observations.

II. EXPERIMENT

One of the goals of this study is to understand the importance of the magnitude and symmetry of applied lattice distortions in stabilizing new magnetic ground states in thin films. To that end, SRO thin films were grown on (100) and (110) $SrTiO_3$ (STO), $(LaAlO_3)_{0.3}(Sr_2AlTaO_6)_{0.7}$ (LSAT), and $LaAlO_3$ (LAO) as well as (111) STO in thicknesses ranging from 15 to 120 nm. This combination of substrates and thicknesses yielded tetragonally, monoclinically, and trigonally distorted films with film-substrate lattice mismatches that varied from -0.64% on STO and -1.8% on LSAT to -3.6% on LAO. Samples were grown using pulsed-laser deposition in 60 mtorr O_2 at a temperature of 700 °C and a laser fluence of approximately 1.3 J/cm^2. They were then postannealed in 100 torr O_2 at 600 °C for 7 min.

SRO has an orthorhombic structure with bulk lattice parameters $a = 5.57$ Å, $b = 5.53$ Å, and $c = 7.84$ Å; however, it can be well represented as a pseudocubic perovskite with $a = 3.93$ Å, which is the structure we will use to describe orientation throughout this paper.[20–22] Structural characterization was performed by x-ray diffraction in the form of ω rocking curves, θ-2θ scans, and reciprocal lattice maps taken on a Panalytical X'Pert materials research diffractometer. Surface morphology was characterized by atomic force microscopy (AFM). Film thickness and stoichiometry were obtained by Rutherford backscattering spectrometry (RBS). Transport measurements were taken in a Quantum Design PPMS system from 4 K to 300 K in magnetic fields of up to 7 T. For magnetic characterization, we used a Quantum Design MPMS-5 SQUID magnetometer varying temperature and applied field. All saturated magnetization values were taken at a temperature of 10 K and an applied field of 5 T. X-ray absorption (XA) and x-ray magnetic circular dichroism (XMCD) spectra, taken at beamlines 4.0.2 and 6.3.1 of the Advanced Light Source at Lawrence Berkeley National Laboratory, were used to test for magnetic impurities such as Fe, Ni, or Co to confirm elemental valence states and to acquire element-specific magnetic information.

III. STRUCTURE AND MORPHOLOGY

Such a systematic study of the effect of lattice distortions requires a set of consistently high-quality samples and accurate characterization of the magnitude of the applied strain. To that end, we utilized a combination of structural and surface-characterization techniques that indicate our SRO films are epitaxial, highly crystalline, stoichiometric, and smooth. Our $\theta - 2\theta$ x-ray diffraction scans indicate high-quality films with peaks corresponding exclusively to SRO and the substrates in the expected crystallographic orientations. Rocking curves of the film peaks showed excellent epitaxy with mosaic spreads as low as 0.038°. Among substrates of a particular orientation, mosaicity is inversely related to lattice mismatch, with films on STO showing smaller mosaic spread than films on LSAT and LAO, which show increasing mosaicity. Films on (100) and (110) STO have much lower mosaic spread than films on (111) STO.

A comparison of reciprocal lattice maps (RLMs) of SRO films grown on different substrates and in different orientations revealed a variety of strain states. By varying lattice mismatch from -0.7% to -3.8% and thickness from 15 to 120 nm we grew films that were coherently strained, partially relaxed, and fully relaxed. RLMs of the films grown on (100) and (110) STO show that films are strained up to thicknesses of 80 nm but begin to show partial relaxation by 120 nm.[15] Films on LSAT begin to relax partially at thicknesses above 60 nm. On LAO, films are difficult to grow fully strained; 40- to 50-nm-thick films are partially relaxed and full relaxation occurs by 80 nm.[16] These fully relaxed films on LAO, as well as the thicker partially relaxed films on STO, can serve as important reference samples. If lattice distortions are controlling the film properties, these films should show much more bulk-like behavior.

It is more difficult to stabilize coherently strained films in the (111) orientation. RLMs of the (321) reflection of films on (111) STO show greater relaxation than films of comparable thickness in other orientations. For SRO films on (111) STO, coherent strain can be maintained only for films less than 30 nm thick. This challenge is magnified in (111)-oriented films on LSAT and LAO and we, therefore, only discuss films grown on (111) STO. In these films on (111) STO, we were able to obtain a variety of different strain states ranging from coherently strained to partially relaxed as film thickness was increased from 15 to 120 nm.

We found additional confirmation of film quality through characterization of surface morphology using AFM and film stoichiometry using RBS. AFM measurements reveal unit cell terraces on the smoothest films on (100) STO that transition to bunched steps for films grown on LSAT and rougher 3D islands on LAO where epitaxial strain is larger. Even these rougher films on LAO had roughnesses much lower than the film thickness. RBS measurements were consistent with $SrRuO_3$, showing a 1 : 1 ratio of Sr and Ru. It is much more difficult to accurately determine O content; all measurements are consistent to within experimental error with the expected stoichiometry. Thus, through a combination of AFM, x-ray diffraction, and RBS, we conclude that we have grown high-quality stoichiometric films of SRO in a wide variety of strain states.

IV. MAGNETISM

Having grown high-quality SRO films in a variety of strain states, we examined the magnetic behavior of the films in order to correlate it with the structure. To examine the relationship among epitaxial strain, enhanced magnetic moment, and magnetic anisotropy, we used SQUID magnetometry to probe the saturated magnetic moment with the field applied in-plane and out-of-plane. We also used XMCD to determine the elemental origin of these effects and elucidate the ratio of spin and orbital contributions to the magnetic moment. We observed enhanced Ru magnetic moment in triclinically distorted (111) films relative to (100) and (110) SRO films, which are themselves enhanced relative to bulk SRO. This enhancement appears to be primarily due to an increase in the spin contribution to the magnetic moment, with a small increase in the orbital contribution as well. Additionally, the easy axes of all compressively strained films are OOP regardless of substrate orientation. Both effects are strongly correlated to lattice distortions imposed by the substrate.

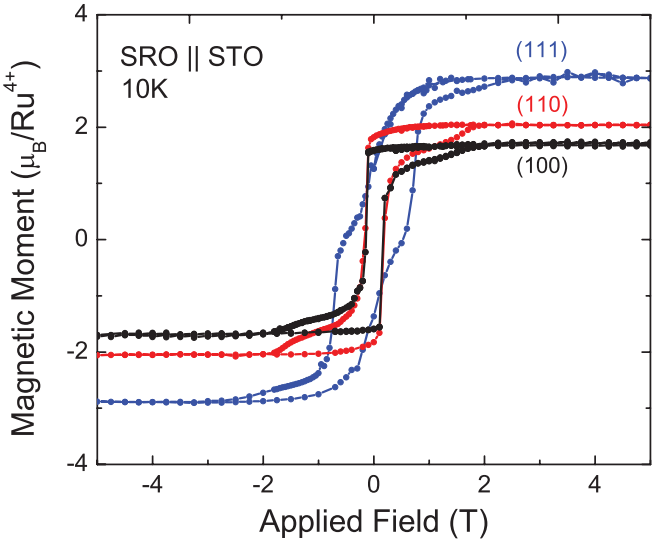

FIG. 1. (Color online) Hysteresis loops taken at 10 K of 60- to 70-nm-thick films on (100)-, (110)-, and (111)-oriented STO showing the strong relationship between strain orientation and saturated moment. It should be noted that the loop of the (111)-oriented film displays a pinched shape characteristic of two magnetic states. This effect is consistent with the stabilization of a mixture of high- and low-spin states.

SQUID magnetometry revealed a strong dependence of the saturated moment on substrate orientation, as illustrated in Fig. 1, which shows a typical series of films between 60 and 70 nm thick on (100)-, (110)-, and (111)-oriented STO. Compressively strained films of all orientations exhibited enhanced saturated magnetic moments compared to previous bulk and thin film values of 1.1–1.6 μ_B/Ru^{4+} regardless of film thickness. On all substrate materials, (110)-oriented films generally had higher-saturated moments than (100)-oriented films. However, all of our (100) and (110) films saturate at or below 2.35 μ_B/Ru^{4+} and can be explained in terms of a low-spin moment of 2 μ_B/Ru^{4+} ions combined with a 10–15% orbital contribution (described later). Our completely relaxed films on (100) LAO showed much more bulk-like behavior, saturating at a magnetic moment of 1.2 μ_B/Ru^{4+}, while the thickest, partially relaxed films on (100) STO had saturated moments of 1.44 μ_B/Ru^{4+}. These observations indicate that our films are quite bulk-like in the absence of strain.

In contrast to (100)- and (110)-oriented films, SQUID magnetometry of SRO in the (111) orientation showed high-saturated moments, which suggest that trigonally distorted (111) SRO films are in a high-spin Ru state characterized by a mix of t_{2g} and e_g states at the Fermi level. Numerous films on (111) STO exhibit values in excess of 2.4 μ_B/Ru^{4+}, with some as high as 3.5 μ_B/Ru^{4+}. Such large moments cannot be explained in terms of a low-spin Ru state. Thus, we can see that the symmetry of the applied lattice distortion, in addition to its magnitude, is crucial in determining the magnetic state.

Within a given orientation, we also observed significant variation between films of different thicknesses and between films on different substrate materials. By growing the (100)-oriented films at varying thicknesses on STO, LSAT, and LAO, we synthesized (100) SRO films with a range of strain states

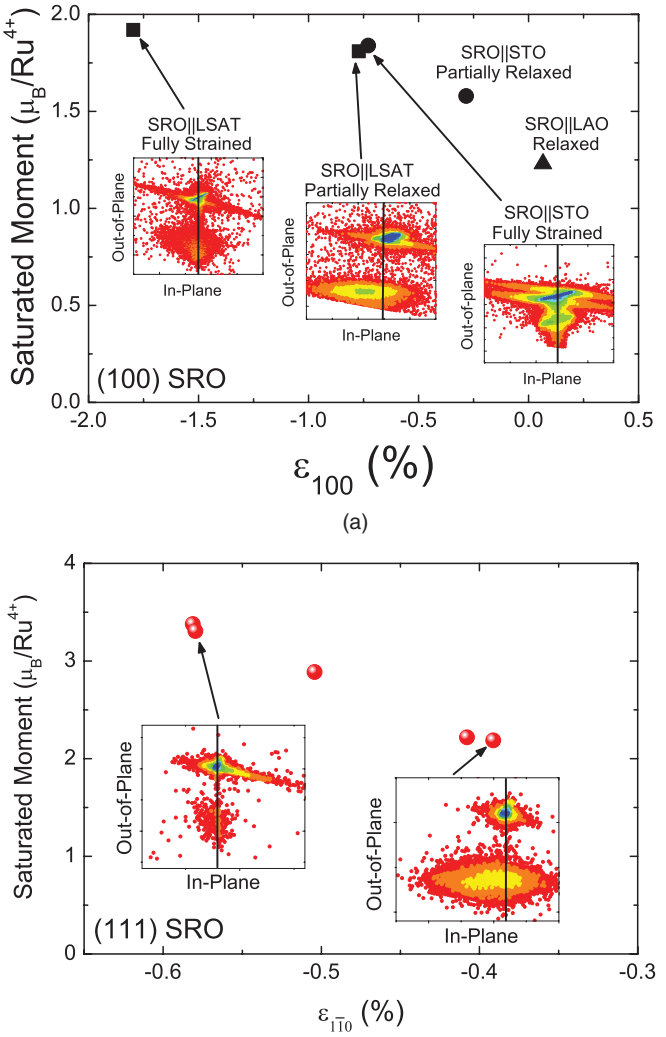

FIG. 2. (Color online) Saturated magnetic moment vs. strain for films on (a) (100)-oriented STO, LSAT, and LAO and (b) (111)-oriented STO. Thicknesses range from 20 to 120 nm. Strain values extracted from the 301 and 312 reflections, respectively, show that as compressive in-plane strain increases, (100)-oriented films approach a saturated magnetic moment of 2 μ_B/Ru^{4+} while (111)-oriented films approach a saturated moment of 4 μ_B/Ru^{4+}. (Insets) RLMs of several films further demonstrate that it is the lattice distortion that determines the magnetic state.

and saturated Ru moments and attempted to correlate the two using RLMs. Although it is straightforward to extract a specific strain from the RLM in a coherently strained film, there is a distribution of film lattice parameters in partially relaxed films that makes it difficult to extract a specific value for strain. Thus, to quantify the lattice distortion, we use the mismatch between the average measured film lattice constant and the bulk lattice constant. The high-single-crystalline quality of the films, indicated by their low mosaic spread, makes this approximation well justified and the calculated strain represents well the degree of relaxation in the film. Figures 2(a) and 2(b) shows strain versus saturated moment in (100)- and (111)-oriented SRO films, respectively, along

with typical reciprocal space maps showing relative amounts of relaxation. In these space maps, alignment of the film and substrate peaks along the in-plane axis indicates a coherently strained film while an offset in the film peak means that total or partial relaxation has occurred. We found that films with larger strains always had higher-saturated magnetic moments. In (111) films, there was a rapid increase in magnetic moment as compressive in-plane strains were increased.

We also observe strong magnetic anisotropy in SRO films with an easy axis away from the plane of the film for all strained samples. The magnetic anisotropy of SRO is known to be relatively complex, with some reports showing an OOP easy axis (normal to the substrate)[23] and others showing the easy axis at a temperature-dependent angle to the film normal.[24] However, our observations agree with and expand on the recent reports that for SRO films grown on both (100) and (110) STO the magnetic easy axis is OOP.[14,18] A comparison of our IP and OOP hysteresis loops shows this to be the case for films in (100), (110), and (111) orientations on multiple substrate materials. Although we have not attempted to resolve the angular dependence in detail, the much higher remnant magnetization found in the OOP direction is indicative of an easy axis. Figures 3(a) and 3(b) show hysteresis loops taken with H IP and H OOP for SRO on (100) STO and (100) LAO, respectively. The film on STO is coherently strained while the film on LAO has relaxed to nearly bulk lattice parameters. Although both exhibit anisotropy, the shape of the IP and OOP loops differ substantially in the strained films but are very similar in the relaxed LAO film. Additionally, the difference between IP and OOP saturated moments is much smaller in the relaxed film. When (100)-oriented films are compared using strains calculated from reciprocal lattice maps, more heavily strained films are always more anisotropic. Figure 4 shows a more direct comparison of the tetragonal distortion and the degree of anisotropy, represented by the ratio of magnetic moments with a 5-T field applied IP and OOP. Again, assuming the strain state is well represented by the peak of the measured reciprocal lattice point, we calculate the tetragonal distortion to be $\epsilon_{OOP} - \epsilon_{IP}$. We can see that the magnitude of the tetragonal distortion strongly correlates with the anisotropy, further corroborating the importance of strain in magnetic anisotropy.

X-ray absorption (XA) measurements performed at beamline 6.3.1 and 4.0.2 of the Advanced Light Source showed the samples to be free of magnetic impurities, such as Fe, Co and Ni, to within the sensitivity of the measurements and confirmed that the magnetism originates primarily on the Ru^{4+}, with

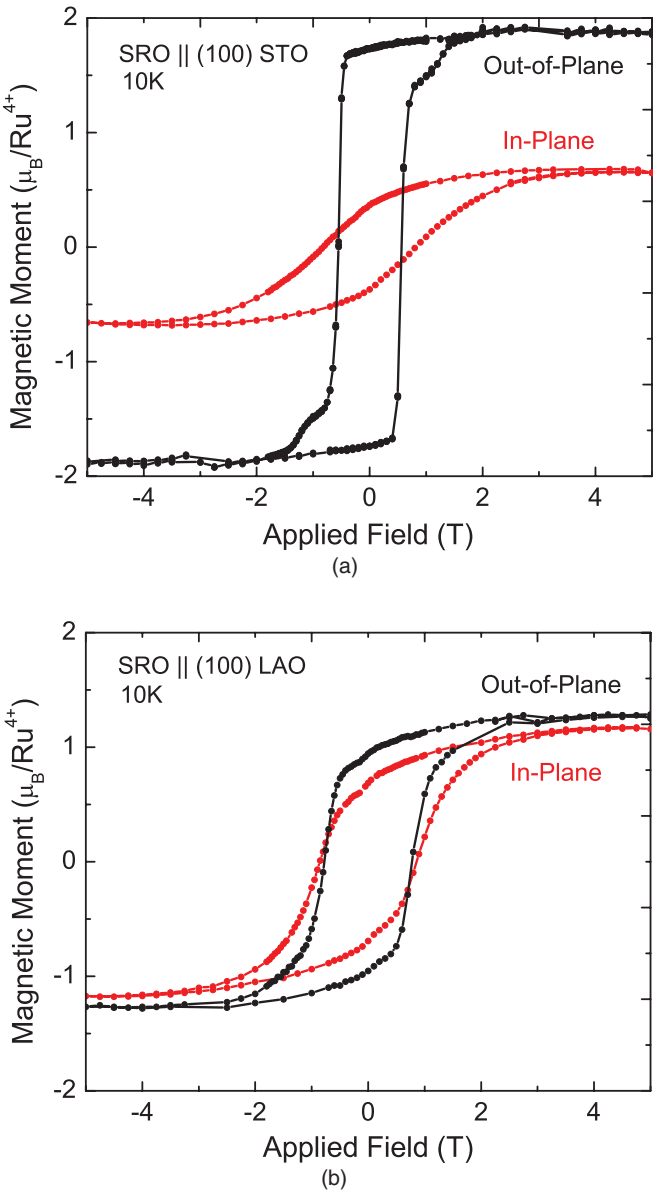

FIG. 3. (Color online) Magnetic moment vs. applied field at 10 K with external field in the in-plane and out-of-plane directions for (a) coherently strained SRO on (100) STO and (b) relaxed SRO on (100) LAO.

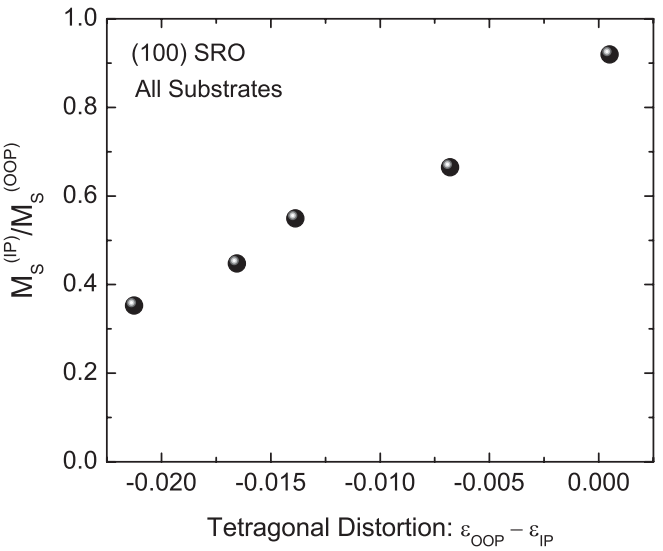

FIG. 4. Anisotropy vs. tetragonal distortion of SRO films grown on (100) STO, LSAT, and LAO at a variety of thicknesses between 20 and 120 nm. Tetragonal distortion was calculated using reciprocal lattice maps, and anisotropy was measured by taking the ratio of film moments in a 5-T field applied in-plane and out-of-plane. Anisotropy can be seen to increase with tetragonal distortion.

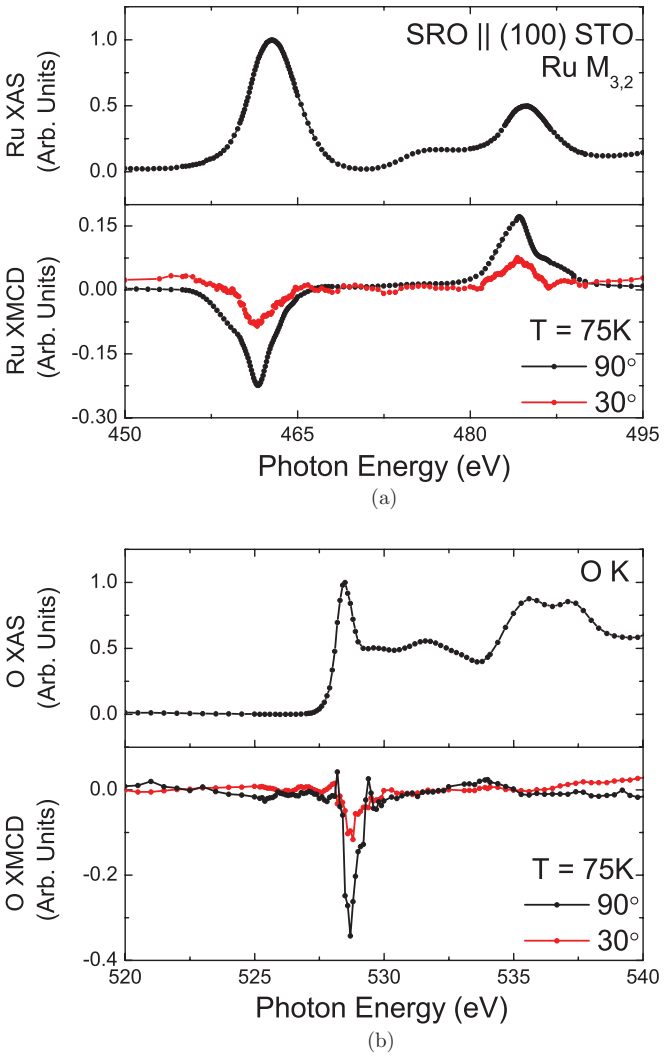

FIG. 5. (Color online) (a) Ru $M_{3,2}$ and (b) O K-edge x-ray absorption (XA) and x-ray magnetic circular dichroism (XMCD) spectra of SRO on STO. The XA spectrum is compatible with an octahedral coordination of Ru^{4+}, while the XMCD shows magnetism originating in the Ru and, to a lesser extent, the O. XMCD taken at normal (90°) and grazing (30°) incidence shows strong anisotropy in agreement with SQUID magnetometry measurements.

a smaller contribution from O^{2-} ions. Typical examples of Ru and O XA spectra can be seen in Fig. 5. As there is no other known example of high-spin Ru, it is not known what the the XA spectra of high-spin Ru should look like. However, the spectra are consistent with previously reported examples of Ru^{4+} in an octahedral environment.[25] Also shown in Fig. 5 are typical XMCD measurements taken at 75 K with an alternating ±0.5 T applied field at normal (90°) and grazing (30°) angles to the film surface, which allow us to confirm the SQUID magnetic anisotropy measurements and probe the origins of the anisotropy. Application of a magnetic field in grazing geometry results in significantly less dichroism from both the O^{2-} and Ru^{4+} ions when the field is applied OOP, showing greater magnetic polarization in the normal geometry. These Ru and O spectra are indicative of an OOP easy axis in agreement with the SQUID magnetic anisotropy measurements. It is interesting to note that the magnetic polarization and anisotropy is present in the O spectra rather than the Ru alone. This is likely the result of strong Ru 4*d*-O 2*p* hybridization. Together the XMCD and SQUID measurements indicate a strong magnetic anisotropy in strained SRO films.

Through careful application of the XMCD sum rules to the spectra, we calculate the ratio between spin and orbital moment of films in a variety of orientations and strain states. This ratio m_l/m_s was then calibrated to saturated moments measured in the SQUID to yield the estimated magnitude of the orbital moment. Measurements on strained (100)-, (110)-, and (111)-oriented samples show that both the ratio m_l/m_s and the absolute value of the orbital moment are significantly larger for strained films on STO than for relaxed films on LAO. The strained films had ratios between 8% and 15%, corresponding to orbital moments between 0.24 and 0.32 μ_B/Ru^{4+} while relaxed films on LAO had much lower values of $m_l/m_s < 5\%$ and $m_l < 0.06\mu_B/Ru^{4+}$. These values are consistent with the earlier estimates of the maximum attainable moment for Ru^{4+} in a low-spin state for (100) and (110) SRO films and also demonstrate that the high-saturated Ru moment of (111)-oriented films cannot be explained by an orbital moment contribution. Finally, the increased OOP orbital moment in the compressively strained films can be expected to increase the strength of the spin-orbit coupling and potentially cause the strong universal anisotropy.

V. TRANSPORT

In an itinerant ferromagnet where the conduction electrons are responsible for the magnetism, changes in the magnetic properties are often accompanied by changes in electron transport. Consequently, we have performed resistivity and Hall effect measurements to provide further insight into the ground state of our SRO thin films. The results show that the variation in magnitude and symmetry of the epitaxial strain has profound effects on the electronic and magnetic ground state. Resistivity (ρ) versus temperature measurements indicate variation of Curie temperature with epitaxial strain. In Hall effect measurements, we see significant changes in the carrier concentration, which may reflect variation in the density of states near the Fermi level.

Our resistivity values are consistent with other high-quality SRO films, with typical values ranging from 190 to 300 Ω-cm at 300 K.[26] The residual resistivity ratio, here defined as the ratio of the resistivity value at room temperature to that at 5 K, was typically between 3.5 and 5; these values are also in good agreement with other high-quality single-crystalline thin films.[26,27] Relaxed films on both (100) and (110) LAO showed the highest resistivity while films on STO and LSAT were significantly lower. In Fig. 6, we see a direct comparison of films grown on all orientations of STO. SRO on (111) STO shows much higher resistivity and residual resistivity than other STO orientations. We attribute these differences to a combination of different microstructural effects and possibly changes in the effective mass due to modified band structure.

Previous studies have shown that epitaxial strain can lower the T_C of (100)-oriented SRO films.[22,28] We correlated the Curie temperatures (T_C) (as determined by the peak in $d\rho/dT$) with the type of distortion imposed by the substrate. Substrate

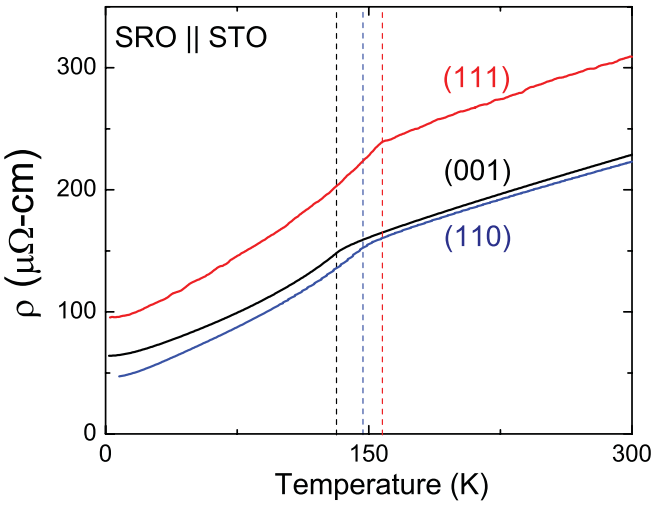

FIG. 6. (Color online) Resistivity (ρ) vs. temperature for 65-nm-thick films on (100), (110), and (111) STO showing significant variation in resistivity and transition temperature among the different orientations. The dashed lines mark the resistivity kink, and, thus, transition temperature, of the corresponding film.

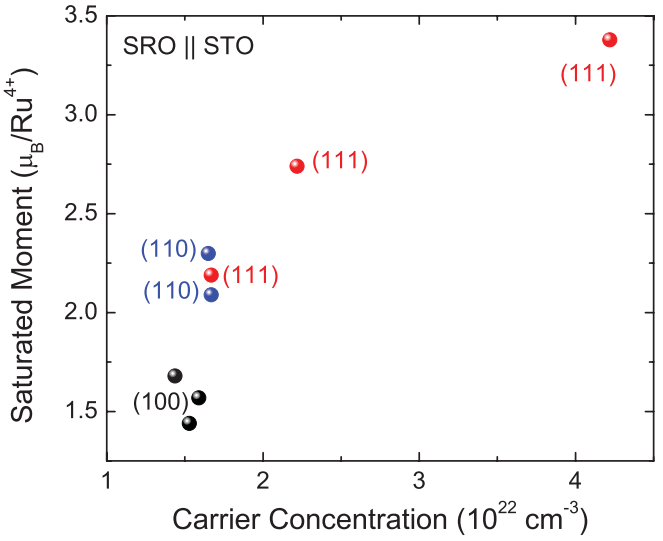

FIG. 7. (Color online) Carrier concentration vs. saturated moment at 50 K for (100)-, (110)-, and (111)-oriented films on STO. Across all different orientations, an increase in carrier concentration is correlated with an increase in saturated magnetic moment.

orientation significantly affected T_C, with typical values of 133–137 K, 142–148 K, and 150–154 K for films on (100)-, (110)-, and (111)-oriented STO, respectively. Films on LSAT and LAO followed similar trends. It is important to note that relaxed films on (100)- and (110)-oriented LAO were much more bulk-like than corresponding films on STO and LSAT, with transition temperatures of 150 K and 156 K, respectively. Although there are a number of factors that affect the T_C of SRO thin films, including stoichiometry and strain magnitude, it is clear that the symmetry of the applied strain is an important factor in determining the strength of the magnetic exchange interaction. Thus, we can see that films in the (111) orientation have the strongest exchange interaction.

Although the Hall effect in SRO exhibits complex temperature-dependent behavior, including a sign change in the vicinity of the Curie temperature,[29–31] we can obtain an estimate of carrier concentration from measurements in the lower-temperature regime (<100 K) using a single band approximation in which $R_{\mathrm{Hall}} = 1/(ne)$. In general, (111)-oriented films have the highest carrier concentrations, with carrier concentrations over twice as large as (100) SRO on STO. It is, at first, surprising that the films with the highest resistivity also have the highest carrier concentration. However, (111) films also exhibit significantly decreased mobility that we believe to be associated with a higher incidence of defects and increased mosaic spread, as observed in residual resistivity and x-ray diffraction measurements, respectively. So, the enhancement of the carrier concentration, and, hence, the density of states at the Fermi level can be correlated with the magnetism. Figure 7 shows the relationship between saturated Ru moments and the carrier concentrations extracted from Hall effect measurements for 30- to 60-nm-thick SRO films on STO of various orientations. Across a variety of orientations of STO with similar thickness, we find that the saturated Ru moment scales with carrier concentration, indicating an enhancement of the density of states at the Fermi level with increasing saturated moment.

VI. DISCUSSION

Correlation of the lattice distortions, enhancement of saturated Ru moment and strong magnetic anisotropy in these SRO films lead us to conclude that it is the symmetry and magnitude of the lattice deformation that produces and controls these unusual magnetic properties. We find the degree of enhancement to be highly tunable and dependent only on the strain state. For example, a partially relaxed film on (100) LSAT whose in-plane lattice parameter is nominally 0.7% smaller than bulk. Its saturated moment is nearly identical to that of a coherently strained film on (100) STO, which is under 0.7% compressive strain (Fig. 4). Both films exhibit saturated moments of 1.8 μ_B/Ru^{4+}. Alternatively, we can use the example of a fully relaxed and partially relaxed pair of films on (100) LAO that saturate at 1.3 and 1.8 μ_B per formula unit, respectively. Thus, two films on different substrates with the same strain have the same saturated moment while two films on the same substrate with different strains have different saturated moments. It is clear, then, that lattice distortions play a dominant role in controlling the magnitude of the saturated moment.

The smaller saturated Ru moment found on (100)- and (110)-oriented films are consistent with a low-spin Ru^{4+} configuration after accounting for the orbital contribution measured with XMCD. However, moment values that greatly exceed 2 μ_B/Ru^{4+} cannot be accounted for within the low-spin Ru^{4+} local moment picture. Through x-ray diffraction and RBS, we have explicitly ruled out the possibility that the additional enhancement is due to factors such as off-stoichiometry or alternate phases. X-ray absorption measurements rule out a change in valence or the presence of magnetic impurities. Finally, XMCD demonstrates that the increase in orbital magnetic moment is much too small to explain the larger effect in (111)-oriented films. Thus, we propose that the pure shear stress of the trigonal distortion imposed by the (111) substrate alters the Ru-O bonds in a way which reduces the splitting between the t_{2g} and e_g orbitals, thus enhancing the density of

states at the Fermi level and effectively stabilizing a high-spin state.

This $t_{2g}^3\ e_g^1$ state would have a maximum saturated moment of 4 μ_B/Ru^{4+}. Since all of our (111) films saturate between 2 and 4 μ_B/Ru^{4+}, it is possible that the high- and low-spin states coexist in thicker, partially relaxed samples where a strain gradient may be present. In fact, we see from Fig. 1 that the hysteresis loops of some (111) films exhibit a "pinching" effect consistent with the coexistence of two distinct magnetic states.

Such a picture is in agreement with the demonstrated relationship between saturated magnetic moment and carrier concentration. If the e_g states are split such that the lower e_g levels become occupied, a corresponding increase in the density of states can be expected. This enhancement of the density of states should manifest itself in an increased carrier concentration, precisely as observed in our films on STO. Moreover, both the carrier concentration and saturated magnetic moment should scale with the density of states at the Fermi level. In this picture, we expect increased carrier concentration to correspond to increased saturated moment, exactly as shown in Fig. 7.

We also can see conclusively from Fig. 4 that the magnetic anisotropy is controlled by the magnitude of the applied lattice distortion. We can estimate the magnitude of the OOP orbital magnetic moment from XMCD measurements. We find that the OOP orbital moment of compressively strained films in all orientations is enhanced relative to bulk-like relaxed films. The Bruno model of magnetocrystalline anisotropy then predicts a corresponding increase in the anisotropy energy of the compressively strained films.[32,33] It is, therefore, likely that the strong magnetic anisotropy is a direct result of enhanced OOP orbital moment in compressively strained films.

These observations provide further corroboration that all of the novel magnetic behavior can be traced back to altered bonding induced by lattice distortions. Bulk SRO is already known to have strong spin orbit coupling relative to most magnetic 3*d* systems, likely due to the relatively heavy Ru ions.[8] However, there are several avenues by which this interaction might be enhanced. Distortions of the Ru-O octahedral could anisotropically reduce orbital overlap and decrease the crystal field splitting. Such a disruption of orbital overlap could reduce the quenching of the orbital moment, leading to strong anisotropy in the orbital moment.

Thus, we see that the anisotropy, enhanced saturated Ru moments, and increases in carrier density are all consistent with a strain-induced stabilization of a high-spin Ru state. We can now form a complete picture of the magnetic state. Compressive strain results in a distortion of the Ru-O octahedra, simultaneously weakening the OOP bonding and splitting the e_g energy levels. The weakened OOP bonding reduces the quenching of the orbital moment and results in strong uniaxial anisotropy while the altered band structure enhances the saturated moment and, in (111)-oriented films, stabilizes a high-spin Ru state.

VII. CONCLUSIONS

In conclusion, we have shown enhanced magnetization in SRO thin films that cannot be explained either by magnetic impurities or an increase in orbital moment. Rather, both magnetic and transport data are strongly indicative of a high-spin state of Ru^{4+}. We have demonstrated that the enhancement of the magnetic moment can be controlled through the application of compressive in-plane epitaxial strain. It is likely that this distortion stabilizes a high-spin state through decreased orbital overlap and a corresponding enhancement in the density of states at the Fermi level by the newly split e_g band. In all cases, the decrease in orbital overlap results in the enhancement of the saturated magnetic moment and universal anisotropy direction even in SRO films of different orientations. This universal anisotropy direction is manifested as an out-of-plane easy axis in all compressively strained films of (100), (110), and (111) orientation and is likely due to the enhancement of the out-of-plane orbital magnetic moment. Finally, we have shown that it is possible to tune the effects of this distortion by varying the orientation and magnitude of this strain, particularly in the case of (111)-oriented films that exhibit evidence of a high-spin Ru^{4+} and the coexistence of two spin states.

ACKNOWLEDGMENTS

We thank J. Rondinelli and N. Spaldin for fruitful discussions and K. M. Yu for his assistance in RBS data collection. This work and the Advanced Light Source are supported by the Director, Office of Science, Office of Basic Energy Sciences, of the US Department of Energy under Contract No. DE-AC02-05CH11231. F. J. W. is supported by the Army Research Office under Grant No. MURI W911NF-08-1-0317.

[1] Y. Moritomo, H. Kuwahara, and Y. Tokura, Physica B **237**, 26 (1997).
[2] R. S. Liu, C. H. Shen, and S. F. Hu, Int. J. Inorg. Mater. **3**, 1063 (2001).
[3] Y. Suzuki, H. Y. Hwang, S-W. Cheong, and R. B. van Dover, Appl. Phys. Lett. **71**, 140 (1997).
[4] D. J. Singh, J. Appl. Phys. **79**, 4818 (1996).
[5] N. Hiraoka, M. Itou, A. Deb, Y. Sakurai, Y. Kakutani, A. Koizumi, N. Sakai, S. Uzuhara, S. Miyaki, H. Koizumi, K. Makoshi, N. Kikugawa, and Y. Maeno, Phys. Rev. B **70**, 054420 (2004).
[6] K. Maiti, Phys. Rev. B **73**, 235110 (2006).
[7] P. B. Allen, H. Berger, O. Chauvet, L. Forro, T. Jarlborg, A. Junod, B. Revaz, and G. Santi, Phys. Rev. B **53**, 4393 (1996).
[8] M. C. Langer, Ph.D. thesis, University of California, Berkeley, 2009.
[9] S. N. Bushmeleva, V. Yu. Pomjakushin, E. V. Pomjakushina, D. V. Sheptyakov, and A. M. Balagurov, J. Magn. Magn. Mater. **305**, 491 (2006).
[10] A. Kanbayasi, J. Phys. Soc. Jpn. **41**, 1876 (1976).
[11] P. S. Anil Kumar, P. A. Joy, and S. K. Date, Physica B **269**, 356 (1999).

[12]D. Toyota, I. Ohkubo, H. Kumigashira, M. Oshima, T. Ohnishi, M. Lippmaa, M. Takizawa, A. Fujimori, K. Ono, M. Kawasaki, and H. Koinuma, Appl. Phys. Lett. **87**, 162508 (2008).
[13]P. Mahadevan, F. Aryasetiawan, A. Janotti, and T. Sasaki, Phys. Rev. B **80**, 35106 (2009).
[14]R. Palai, H. Huhtinen, J. F. Scott, and R. S. Katiyar, Phys. Rev. B **79**, 104413 (2009).
[15]A. Grutter, F. Wong, E. Arenholz, M. Liberati, A. Vailionis, and Y. Suzuki, Appl. Phys. Lett. **96**, 082509 (2010).
[16]A. Grutter, F. Wong, E. Arenholz, M. Liberati, and Y. Suzuki, J. Appl. Phys. **107**, 09E138 (2010).
[17]M. Bohra, C. P. Wu, H. J. Yeh, Y. H. Cheng, C. C. Peng, and H. Chou, J. Appl. Phys. **109**, 07D728 (2011).
[18]X. W. Wang, Y. Q. Zhang, H. Meng, Z. J. Wang, D. Li, and Z. D. Zhang, J. Appl. Phys. **109**, 07D707 (2011).
[19]A. T. Zayak, X. Huang, J. B. Neaton, and K. M. Rabe, Phys. Rev. B **77**, 214410 (2008).
[20]C. W. Jones, P. D. Battle, P. Lightfoot, and W. T. A. Harrison, Acta Crystallogr. Sect. C **45**, 365 (1988).
[21]C. B. Eom, R. J. Cava, R. M. Fleming, J. M. Phillips, R. B. van Dover, J. H. Marshall, J. W. P. Hsu, J. J. Krajewski, and W. F. Peck Jr., Science **258**, 1766 (1992).
[22]Q. Gan, R. A. Rao, C. B. Eom, J. L. Garrett, and M. Lee, Appl. Phys. Lett. **72**, 978 (1998).
[23]L. Klein, J. S. Dodge, T. H. Geballe, A. Kapitulnik, A. F. Marshall, L. Antognazza, and K. Char, Appl. Phys. Lett. **66**, 2427 (1995).
[24]M. Ziese, I. Vrejoiu, and D. Hesse, Phys. Rev. B **81**, 184418 (2010).
[25]J. Okamoto, T. Okane, Y. Saitoh, K. Terai, S.-I. Fujimori, Y. Muramatsu, K. Yoshii, K. Mamiya, T. Koide, A. Fujimori, Z. Fang, Y. Takeda, and M. Takano, Phys. Rev. B **76**, 184441 (2007).
[26]Q. X. Jia, F. Chu, C. D. Adams, X. D. Wu, M. Hawley, J. H. Cho, A. T. Findikoglu, S. R. Foltyn, J. L. Smith, and T. E. Mitchell, J. Mater. Res. **11**, 2263 (1996).
[27]W. Siemons, G. Koster, A. Vailionis, H. Yamamoto, D. H. A. Blank, and M. R. Beasley, Phys. Rev. B **76**, 075126 (2007).
[28]Y. J. Chang, J. I. Kim, and C. U. Jung, J. Magnetics **13**, 61 (2008).
[29]S. C. Gausepohl, Mark Lee, R. A. Rao, and C. B. Eom, Phys. Rev. B **54**, 8996 (1996).
[30]Yevgeny Kats, Isaschar Genish, Lior Klein, James W. Reiner, and M. R. Beasley, Phys. Rev. B **70**, 180407 (2004).
[31]M.-H. Kim, G. Acbas, M.-H. Yang, M. Eginligil, P. Khalifah, I. Ohkubo, H. Christen, D. Mandrus, Z. Fang, and J. Cerne, Phys. Rev. B **81**, 235218 (2010).
[32]P. Bruno, Phys. Rev. B **39**, 865 (1989).
[33]G. van der Laan, J. Phys.: Condens. Matter **10**, 3239 (1998).